Coherent vortex structures over a rotating spinner under non-axial inflows at low Reynolds number

Tambe, Sumit; Schrijer, Ferdinand; Gangoli Rao, Arvind; Veldhuis, Leo

Publication date
2019

Document Version
Accepted author manuscript

Published in
54th 3AF International Conference AERO2019 At: Paris, France

Association Aéronautique et Astronautique de France

54th 3AF International Conference on Applied Aerodynamics
25 – 27 March 2019, Paris - France

FP45-AERO2019-Tambe

COHERENT VORTEX STRUCTURES OVER A ROTATING SPINNER UNDER NON-AXIAL INFLOWS AT LOW REYNOLDS NUMBER

Sumit Tambe [(1)] , Ferry Schrijer [(2)] , Arvind G Rao [(3)] and Leo Veldhuis [(4)]
[(1)] FPP, AWEP, Aerospace Engineering, TU Delft, Kluyverweg 1, 2629HS, Delft, The Netherlands, Email:s.s.tambe@tudelft.nl
[(2)] Aerodynamics, AWEP, Aerospace Engineering, TU Delft, Kluyverweg 1, 2629HS, Delft, The Netherlands, Email:f.f.j.schrijer@tudelft.nl
[(3)] FPP, AWEP, Aerospace Engineering, TU Delft, Kluyverweg 1, 2629HS, Delft, The Netherlands, Email:A,GangoliRao@tudelft.nl
[(4)] FPP, AWEP, Aerospace Engineering, TU Delft, Kluyverweg 1, 2629HS, Delft, The Netherlands, Email: L.L.M.Veldhuis@tudelft.nl

ABSTRACT

Boundary layer instabilities and the formation of coherent spiral vortices over a rotating cone and ellipsoid are studied experimentally. It is found that under a non-axial inflow, the breaking of symmetry in the flow field significantly disturbs the coherence and delays the formation of spiral vortices to higher local Reynolds numbers (Re_l) and higher rotation ratios (S). Consequently, it also delays boundary layer transition region. A conceptual reasoning for the observed phenomena is given based on the sensitivity of the local spiral vortex characteristics (number n and angle ϵ) to the asymmetry in the local rotation ratios.

1. INTRODUCTION

Concepts of novel aircraft configurations often feature engines embedded in the airframe, ingesting the airframe boundary layer. In other words, these engines are now placed under a continuous off-design conditions. Ingestion of a non-uniform boundary layer creates off-design incidence angles on the transonic fan. The fan itself creates a region of higher suction on the slow moving fluid (lower total pressure). This leads to an upstream re-distribution of the flow and results in a non-axial inflow over the spinner, which contributes to the distortion near the hub [1]. Stall and viscous losses at the blade root near the hub are sensitive to the state of the oncoming boundary layer over the spinner. Therefore, It is important to study the boundary layer development over the spinners under non-axial inflows.

It is known from the studies of [2]–[4] that the boundary layer transition mechanism over the rotating bodies of revolution is governed by spiral vortices that wrap around the surface. Characteristics of these vortices like, wavelength (spacing), angle, Reynolds numbers corresponding to their formation, amplification and breakdown are dependent on the local rotation ratio $S = r\omega/U_e$, where r is the local radius, ω is the angular velocity of a body and U_e is the velocity at the edge of the boundary layer. However, all of these studies are limited to the case of still fluid or axial inflow. Therefore, the present study is focused on extending the conditions to the case of a non-axial inflow.

In the present study, the boundary layer instability and coherent structures over a rotating cone and ellipsoid (as they are closer representatives of spinners) are studied using experiments at relatively low inflow Reynolds number $Re_D = 7.4 \times 10^3 \; to \; 2 \times 10^4$ and at various rotation ratios $S_b = r\omega/U_\infty = 0 \; to \; 5$ (U_∞ is the freestream velocity and D is the base diameter). The effect of non-axial inflow is introduced by changing the incidence angle. The case of a rotating cone is addressed more in depth as it is well studied in the literature [3]–[6] for the axial inflow cases.

2. EXPERIMENTAL SETUP

Experiments are performed in a low speed wind tunnel (W-tunnel) at the Faculty of Aerospace Engineering, TU Delft. The wind tunnel is used in an open jet configuration having a cross section of $60 \times 60\ cm^2$. Infrared thermography, using a CEDIP FLIR SC7300 Titanium IR camera, is used to capture the temperature footprint of the spiral vortices on the model surface. Since it is not essential to have the actual temperature in terms of degrees, no camera calibration is performed and the values are given in terms of the digital pixel intensity I'. The levels of temperature fluctuations observed are below $1.3K$. The IR camera was recording at a frequency of 200 Hz, which was sufficient to track the vortex evolution in time. Two geometries are investigated, a cone and an ellipse, which are mounted on a sting and are rotated at $5000\ RPM$ by use of a brushless motor. The sting is attached to a mechanism which allows changing the incidence angle. The model surface is heated by a light source to increase the thermal contrast. The models are made of Polyoxymethylene as it has favourable thermal properties for this application (especially low thermal conductivity). Both the cone and ellipse have same base diameter (D) of $47mm$. The cone has the half angle $\psi = 15^0$, whereas, the ratio of major to minor axis of an ellipse is equal to 2.

Time resolved Particle Image Velocimetry (PIV) is performed in a symmetry plane using 2 high speed cameras (Photron Fastcam SA-1) in stereo configuration and 1 high speed camera in planar configuration.

Data from IRT is post processed using POD analysis. The azimuthal number of vortices $(n \geq 8)$ is used as a lower bound to select the physical admissibility of the POD modes. The reconstruction shows the structure of the spiral vortices. Further, RMS of I' is used to identify the transition region. PIV data is used to obtain the boundary layer edge velocity.

3. OVERVIEW OF FLOW FIELD

Previous studies show two types of instabilities that lead to the formation of spiral vortices in a laminar boundary layer over a rotating body. The first is a cross flow instability which occurs on rotating cones with half angle $\psi > 30^o - 40^o$ and leads to the formation of co-rotating spiral vortices [7]. For $\psi < 30^o - 40^o$ the centrifugal (Görtler) instability dominates and counter-rotating spiral vortices are formed. The present study deals with the latter. In the case of inflow, these vortices are convected downstream where they grow, amplify and break-down. This enhances mixing process in the boundary layer and makes it unstable. This unstable boundary layer undergoes transition to a turbulent state [5]. Vortex characteristics, such as, the angle (ϵ), the azimuthal number (n) depend on S. However, the transition process is also dependent on the Reynolds number Re_l. The coordinate system used in the present study is shown in Figure *1*.

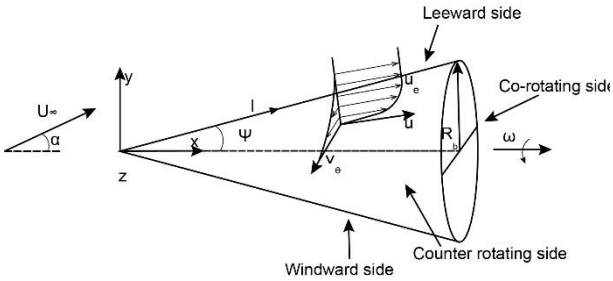

Figure 1 Cartesian coordinate system used in the present study.

4. AXIAL INFLOW

First the case of axial inflow over a rotating cone is addressed which can be considered as a reference for comparison with non-axial conditions. Figure *2* shows the development and amplification of the spiral vortices in the case of an axial inflow. On the left is the trace of I' along the $y/D = 0$ in an instantaneous image and corresponding RMS (dashed line) over the dataset. On the right is the corresponding I' field showing the footprints of the vortex structure. We can observe that at first a relatively strong patch of vortices is about to enter a region of high RMS. As it travels downstream, it undergoes a sudden amplification in the strength, through, what appears to be a vortex pairing. Based on this observation, we can define two points in the graph of RMS I'. The first point, located at l_c, is defined as a critical point at which the vortices start to undergo amplification (where RMS starts growing). Corresponding critical Reynolds number is defined as $Re_{l,c} = l_c U_e/\nu$, where, ν is the kinematic viscosity of air. The second point, located at l_m is related to the peak of amplification (peak RMS), and is defined as the maximum amplification Reynolds number $Re_{l,m} = l_m U_e/\nu$. Figure *3* shows the comparison of both Reynolds numbers with the experimental and theoretical data from the literature [3]. The grey lines in Figure *3* indicate how the Re_l varies with respect to S as we move downstream on the cone from the tip to the base. It is observed that the values of $Re_{l,m}$ from the present measurements are in a good agreement with the values from the theoretical predictions from the literature. Also, the trend of $Re_{l,c}$ is in good agreement and the present data is a bit closer to the theoretical predictions than the

past experimental data. The discrepancy between measured and theoretical data of critical Reynolds number is due to the limited sensitivity of the experiments. Measurements from past experiments were done with a hot wire which can only go down to a limited distance from the wall. Therefore, it can only observe the vortices once they have grown up to a certain size. However, the present data is obtained from the measurements at the wall and that is why it can better detect the inception of the vortices and thus is closer to the theoretical predictions compared to the past experiments. However, it still is limited by the sensitivity of the camera towards the small temperature fluctuations. Nevertheless, it shows that the RMS I' gives a reliable estimation of $Re_{l,c}$ and $Re_{l,m}$.

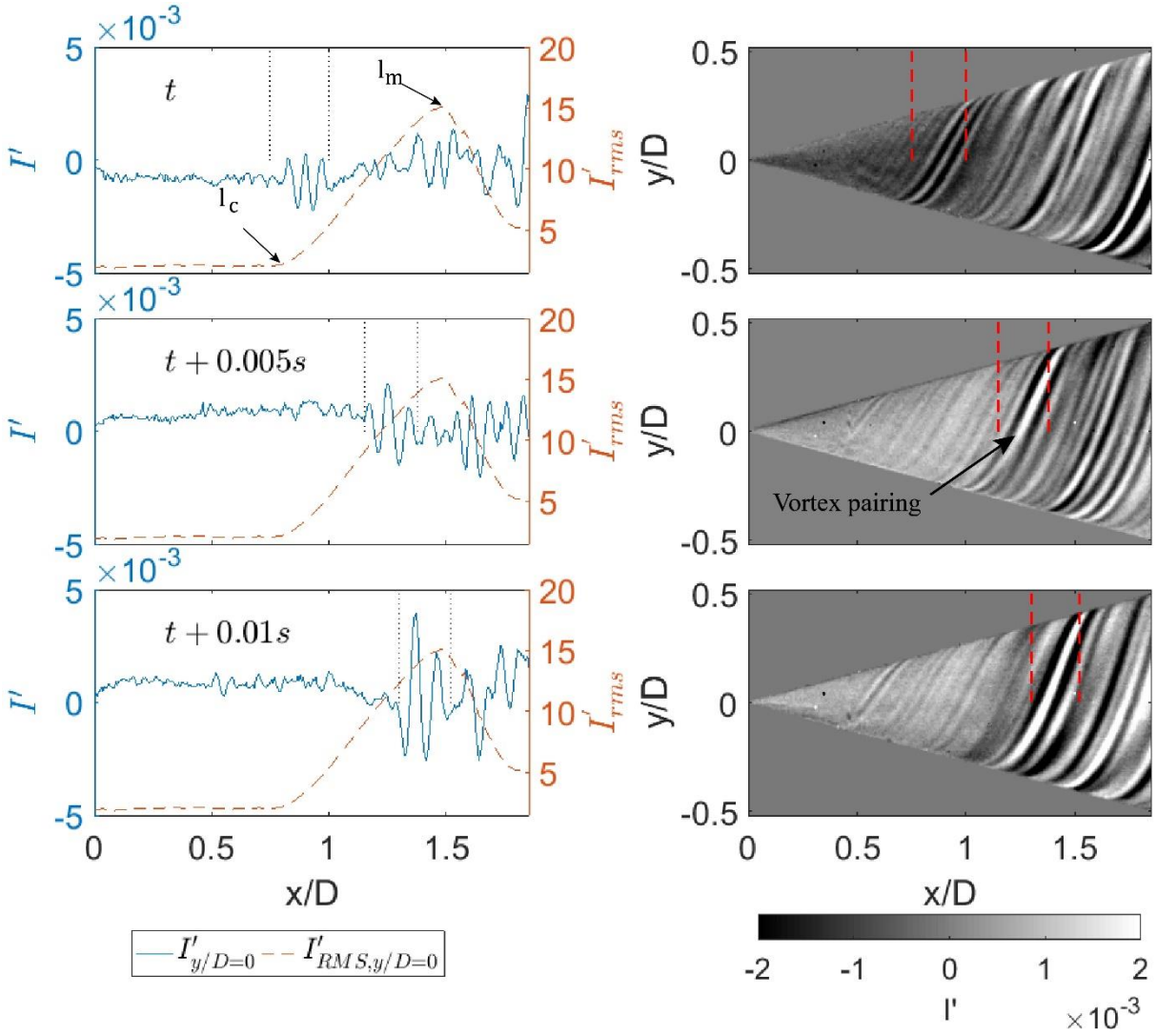

Figure 2 Development and amplification of spiral vortices in axial inflow ($S_b = 3.5$, $Re_D = 1.1 \times 10^4$, $S = 0 - 3.3$, $Re_l = 0 - 2.25 \times 10^4$).

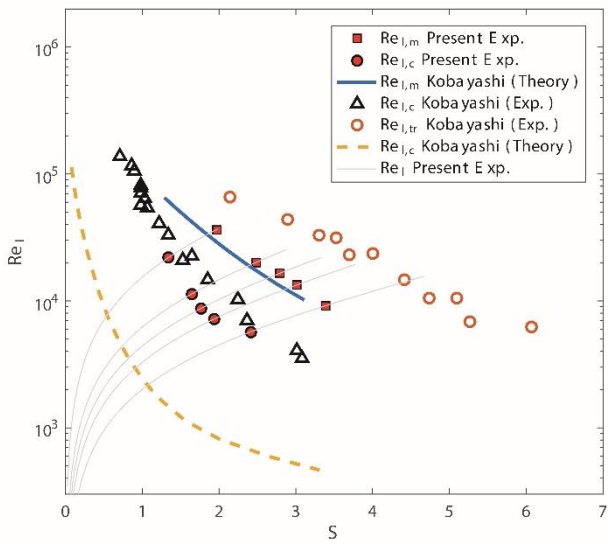

Figure 3 Comparison of $Re_{l,c}$ and $Re_{l,m}$ with the data from literature [3]

5. NON-AXIAL INFLOW

Even a small incidence angle has been observed to have a significant effect on the formation and growth of the coherent spiral vortices. Consequently, this also affects the whole transition region. Figure *4* shows the cases with an incidence angle of $\alpha = 2^o$. It can be observed that even for such a small incidence, the formation of the spiral vortices is delayed downstream (or at a higher S) as compared to the case of an axial inflow. A critical reader might doubt that this could be an artefact of the measurement technique. But we show here results for two inflow Reynolds numbers. It can be observed that with increased Reynolds number the RMS field is also pushed downstream on the cone for the exact same experimental arrangement. Therefore, it can be concluded that the formation of the coherent vortices itself is delayed. Consequently, it also delays the amplification of these vortices. Similar behaviour is observed for increasing incidence angles as shown in the Figure *5*.

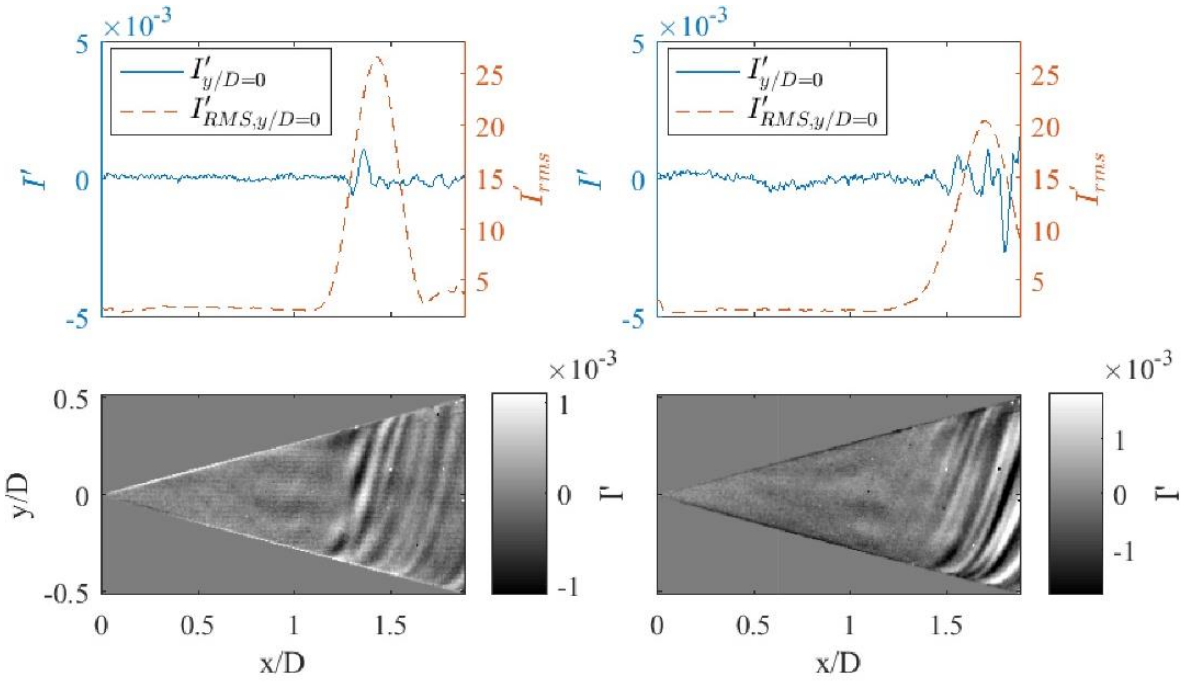

Figure 4 Effect of an incidence angle on the spiral vortices at $\alpha = 2^o$ for two different inflow velocities. $U_\infty = 2.46\ m/s$, $S_b = 5$, $Re_D = 7.7 \times 10^3$ (left) and $U_\infty = 3.51\ m/s$, $S_b = 3.5$, $Re_D = 1.1 \times 10^4$ (right).

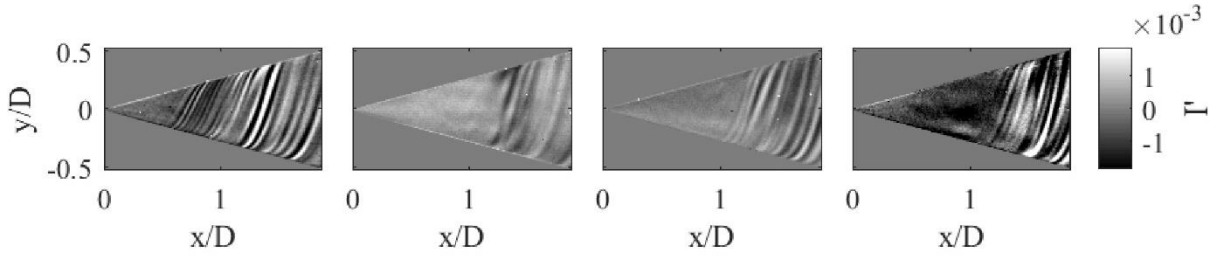

(a) (b) (c) (d)

Figure 5 Delayed formation of the coherent spiral vortices under an incidence angle (a) $\alpha = 0^o$, (a) $\alpha = 2^o$, (a) $\alpha = 4^o$ and (a) $\alpha = 10^o$, ($S_b = 5, Re_D = 7.7 \times 10^3$).

Figure 6 shows the critical ($Re_{l,c}$) and maximum amplification ($Re_{l,m}$) Reynolds numbers for the cases with different incidence angles and inflow Reynolds numbers. Note that these Reynolds numbers are computed with the scaling (edge velocity field) from the axial inflow case. However, the velocity field itself is asymmetric and therefore the local values of S and Re_l are distributed in a highly asymmetric manner around the cone. Figure 7 shows $Re_{l,m}$ and S obtained using the local boundary layer edge velocity for one case of inflow Reynolds number. It can be observed that the trend is not altered significantly from the trend in Figure 6.

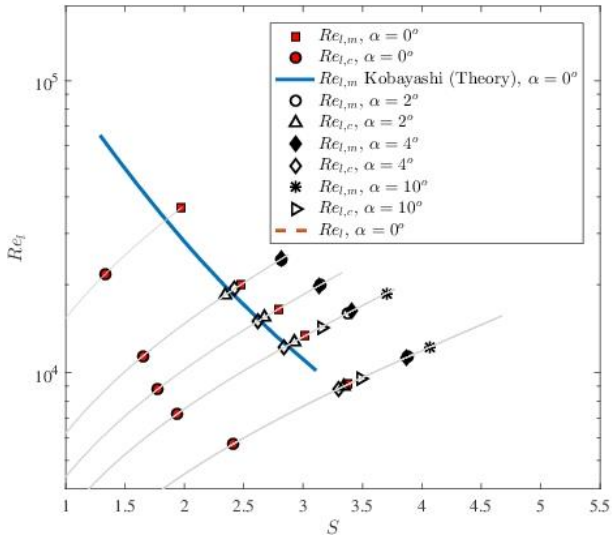

Figure 6 Effect of an incidence angle on the $Re_{l,c}$ and $Re_{l,m}$.

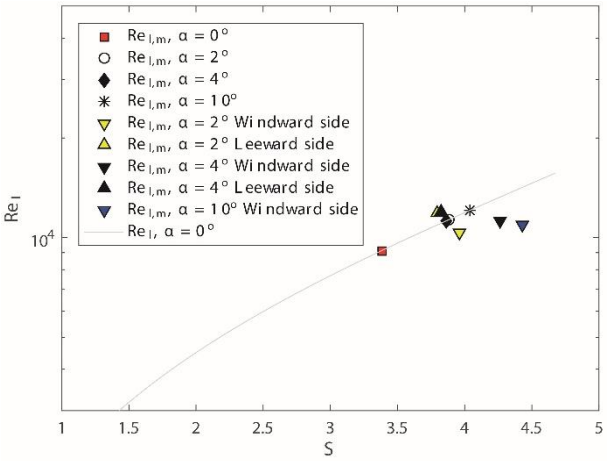

Figure 7 $Re_{l,m}$ and S obtained using the local values of the boundary layer edge velocity.

Conceptual consideration

The aforementioned observations can be explained by addressing the asymmetry in the flow field. By introducing the incidence angle, there are two contributions that affect the symmetry. First, the boundary layer edge velocity on the windward side is much lower than on the leeward side (see Figure 8). This results in different values for Re_l and S at the same axial location. On the other hand, the co and counter rotating sides have a significantly different tangential velocity profile (see Figure 9). Relative to the outer flow, the cone surface has a higher tangential velocity on the counter-rotating side and therefore the apparent rotation ratio, S, will be locally high. However, on the co-rotating side, the relative velocity of the cone and consequently the local S will be lower.

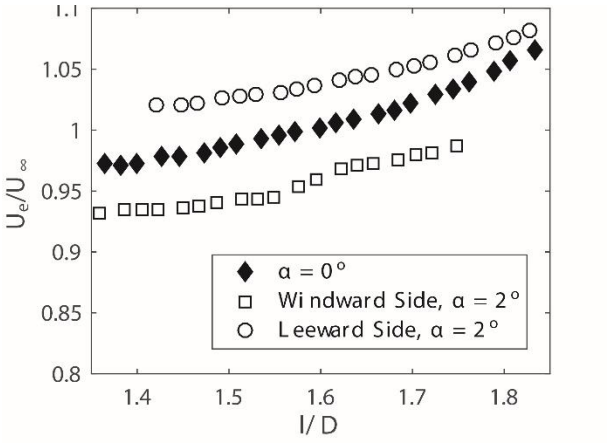

Figure 8 Asymmetry in the boundary layer edge velocity, caused by an incidence angle.

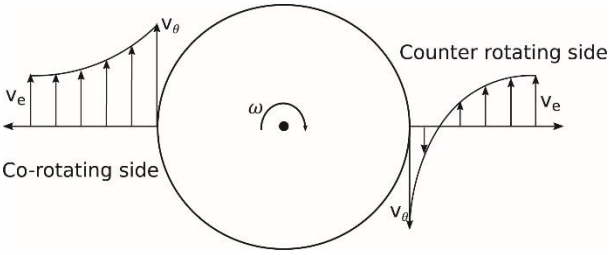

Figure 9 Asymmetry in the counter and co-rotating sides.

These asymmetries have a combined effect on the varying distribution of S and Re_l along the circumference at a fixed axial location. This has a direct effect on which wavelengths will grow to form a coherent spiral vortex structure. It is known from the past studies that the azimuthal number of spiral vortices (n) and the angle (ϵ) is a function of S. n can be related to the azimuthal wavelength $\lambda_\theta = 2\pi r/n$, and together with ϵ, it can be used to compute the overall wavelength of the spiral vortices. As seen from Figure 10 and Figure 11, the slope of the graphs (especially n vs S) are steeper at lower S and reduce in magnitude for increasing S until it reaches the asymptote at $S \to \infty$. This means that any small variation in S at lower S will have a significant effect on n and ϵ, but it will result in much lower change at larger values of S. Note, that on the cone S is zero at the nose and increases downstream. In the case with an incidence angle, even though the boundary layer might be unstable at lower overall S, different wavelengths $(\lambda_\theta, \epsilon)$ tend to grow locally at different parts of the circumference. This way no single wavelength can grow to form a coherent vortex structure until a point where S is large enough so that the variations in n and ϵ has become relatively insignificant. This conceptually explains that by breaking the symmetry in the flow field coherent spiral vortices are formed further downstream on the model.

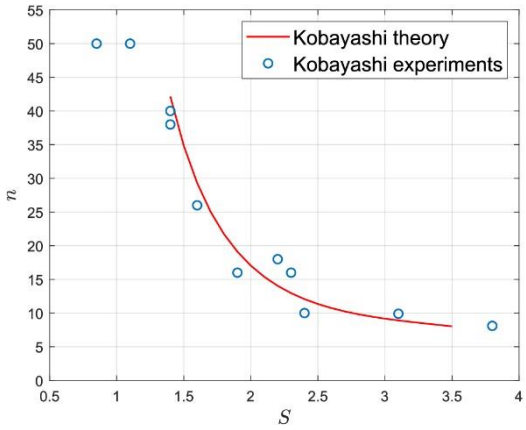

Figure 10 Number of spiral vortices vs rotation ratio, adapted from [3].

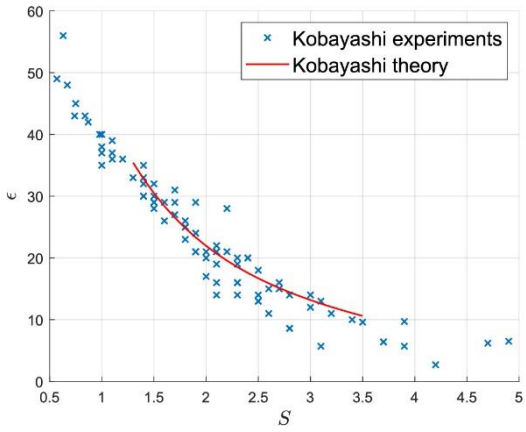

Figure 11 Spiral vortex angle vs rotational ratio, adapted from [3].

6. ROTATING ELLIPSOID

A second geometry that has been investigated is a rotating ellipsoid under the incidence angle. Figure 12 shows the effect of the incidence angle on the instantaneous vortex structure on the rotating ellipsoid. Here, we observe a similar delayed formation of the coherent vortices as for the rotating cone. However, the geometry of the ellipsoid is different from that of the cone in the fact that it imposes a pressure gradient due to the surface curvature. The delayed vortex formation is also evident from the traces of intensity along $y/D = 0$ as shown in Figure 13. Even though the reasoning presented in the text earlier is valid here, a further detailed study is necessary .

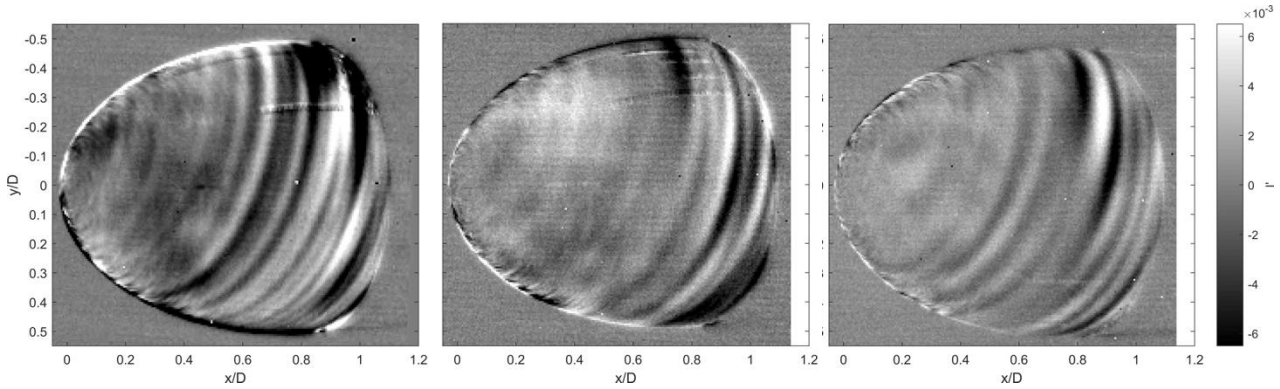

(a) (b) (c)

Figure 12 Instantaneous reconstruction (using 5th to 50th POD modes) of the spiral vortices on the rotating ellipsoid (a) $\alpha = 0^o$, (b) $\alpha = 10^o$ counter rotating side, and (c) $\alpha = -10^o$ co-rotating side. ($S_b = 5, Re_D = 7.7 \times 10^3$).

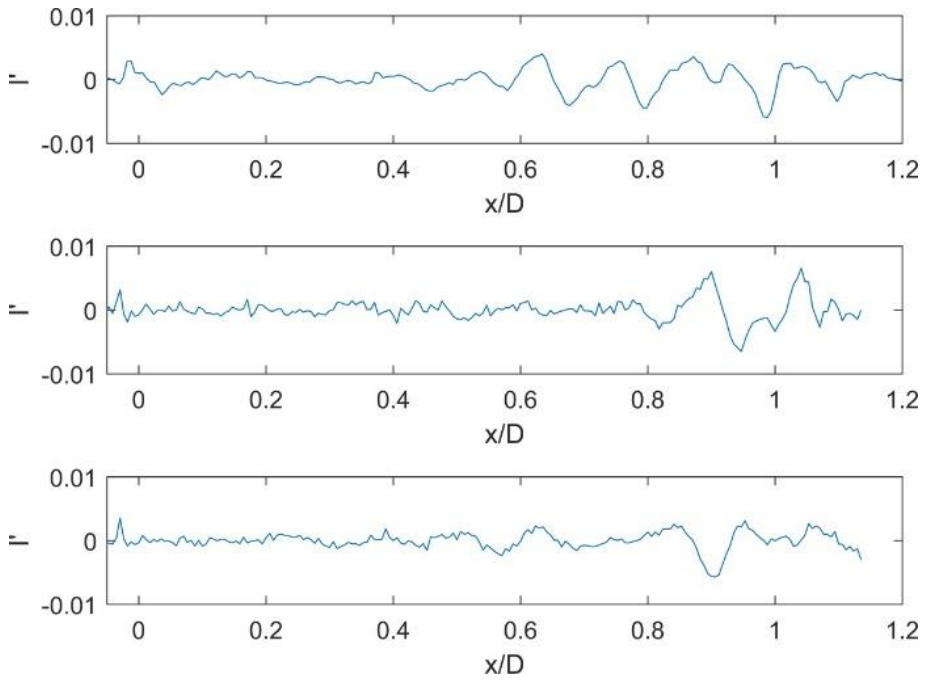

Figure 13 Trace of intensity fluctuations along $y/D = 0$ (a) $\alpha = 0^o$, (b) $\alpha = 10^o$ counter rotating side, and (c) $\alpha = -10^o$co-rotating side. ($S_b = 5, Re_D = 7.4 \times 10^3$).

7. CONCLUSION

The boundary layer instabilities and formation of coherent spiral vortices is studied for axial as well as non-axial case. In the case of a rotating slender cone, the present experimental data of critical and maximum amplification Reynolds number is in the agreement with the past experiments. It has been observed, that the breaking of symmetry has a significant effect on the formation of the coherent spiral vortices. It delays the formation and therefore the whole transition region to the higher Reynolds number and rotation ratios (S). A conceptual reasoning is given based on the sensitivity of the local vortex characteristics (n, ϵ) with the S. At lower S, asymmetry in the local S tends to form vortices with significantly different local characteristics. Therefore, no single wavelength can grow to form a coherent vortex structure. However, at higher S, vortex characteristics are less sensitive to the asymmetry in S and therefore we observe the formation of the coherent vortex structure.

Similar behaviour is observed in the case of a rotating ellipsoid.

8. REFERENCES

[1] V. Jerez Fidalgo, C. A. Hall, and Y. Colin, "A Study of Fan-Distortion Interaction Within the NASA Rotor 67 Transonic Stage," *J. Turbomach.*, vol. 134, no. 5, pp. 369–380, 2010.

[2] R. Kobayashi and H. Izumi, "Boundary-layer transition on a rotating cone in still fluid," *J. Fluid Mech.*, vol. 127, pp. 353–364, 1983.

[3] R. Kobayashi, Y. Kohama, and M. Kurosawa, "Boundary-layer transition on a rotating cone in axial flow," *J. Fluid Mech.*, vol. 127, pp. 353–364, 1983.

[4] R. Kobayashi, "Review: laminar-to-turbulent transition of three-dimensional boundary layers on rotating bodies," *J. Fluids Eng.*, vol. 116, no. 2, pp. 200–211, 1994.

[5] Y. Kohama, "Behaviour of spiral vortices on a rotating cone in axial flow," *Acta Mech.*, vol. 51, no. 3–4, pp. 105–117, 1984.

[6] S. J. Garrett, Z. Hussain, and S. O. Stephen, "Boundary-Layer Transition on Broad Cones Rotating in an Imposed Axial Flow," *Aiaa J.*, vol. 48, no. 6, pp. 1184–1194, 2010.

[7] S. J. Garrett, Z. Hussain, and S. O. Stephen, "The cross-flow instability of the boundary layer on a rotating cone," *J. Fluid Mech.*, 2009.